PHYSICAL REVIEW A **91**, 051801(R) (2015)

Attosecond pulses generated by the lighthouse effect in Ar gas

Valer Tosa,[1,*] Ji Su Lee,[2,3] Hyung Taek Kim,[3,4] and Chang Hee Nam[3,5]
[1]*National Institute for R&D of Isotopic and Molecular Technologies, 400293 Cluj-Napoca, Romania*
[2]*Department of Physics, KAIST, Daejeon 305-701, Republic of Korea*
[3]*Center for Relativistic Laser Science, Institute for Basic Science (IBS), Gwangju 500-712, Republic of Korea*
[4]*Advanced Photonics Research Institute, GIST, Gwangju 500-712, Republic of Korea*
[5]*Department of Physics and Photon Science, GIST, Gwangju 500-712, Republic of Korea*
(Received 6 March 2015; published 7 May 2015)

We numerically investigate harmonic generation in Ar gas under high ionization conditions and demonstrate that a lighthouse effect is present. We examine the structure of the driving field during propagation in temporal, spectral, and spatial domains, and conclude that the complete depletion of neutral Ar on axis gives rise to additional wavelets at off-axis regions. We show that these wavelets propagate with increasing divergence as the radial distances from the axis increase, generating the rotation of the wave front, thus fulfilling a necessary condition for the lighthouse effect. We obtain attosecond bursts of light emitted with different divergences in successive optical half-cycles so that in the far field these bursts arrive at different distances from the beam axis.

DOI: 10.1103/PhysRevA.91.051801 PACS number(s): 42.65.Ky, 32.80.Wr, 42.65.Re, 42.65.Jx

I. INTRODUCTION

The generation of attosecond pulses is a very active research field as these pulses enable the investigation of the light-matter interaction at the atomic unit of the time scale [1]. High-order harmonic generation (HHG) in gas media has been the main method for attosecond pulse generation and photoelectron spectroscopy. In the HHG process an outer shell electron of an atom or molecule is extracted by the strong electric field of a laser pulse, then accelerated in this oscillating field, and, when recombined with the parent atom, releases in a single photon the whole kinetic energy acquired in the driving field. Depending on the experimental conditions, attosecond pulses are generated either as attosecond pulse trains (two bursts in a driving field period) or single attosecond pulses (SAPs). In particular, the single attosecond pulse is desirable to investigate the electronic dynamics of atoms or molecules because it can be applied to directly record the temporal evolution of electron states without side effects from the train of pulses. The generation of a single attosecond pulse, however, requires sophisticated laser technologies, such as single-cycle pulse generation and carrier-to-envelope phase (CEP) control.

A recent and interesting alternative for obtaining a SAP is to create the experimental conditions for the attosecond lighthouse (LH) effect in which consecutive bursts are emitted from the interaction region in well-separated directions, in this way creating a sequence of single attosecond pulses. Lighthouse emission was predicted [2] to occur when inducing a spatial chirp in the laser emission by a slight rotation of one of the gratings in the compressor of a chirped-pulse amplification laser. A different method proposed in the same paper [2] was to introduce an adequate prism in the beam. In both cases the wave-front rotation is considered to be the key condition for the LH effect to occur. Experimentally, the effect was demonstrated by applying the first method to attosecond pulses produced in the laser interaction with a solid-density plasma [3]. Recently, the lighthouse effect was demonstrated in gas-phase HHG [4] by introducing a misaligned pair of glass wedges in the laser beam, which leads to a spatial chirp at the focus. The consequence was that the attosecond pulses generated in successive half-cycles of the laser pulse propagate along different directions from the interaction region.

In gas-phase HHG interesting effects can be seen in the characteristics of the harmonics due to the propagation effects induced in the driving field(s) characteristics, mainly by gas ionization. In Ref. [5] an intense supercontinuum was observed in the range from 35 to 50 eV in a 10-mm-long cell filled with krypton gas and illuminated with 800 nm, 11 mJ, 35 fs pulses. The dramatic changes in the spectral and temporal properties of the driver pulses indicate that propagation effects play a significant role in extreme ultraviolet (EUV) supercontinuum generation. Efficient generation of isolated 160 as (attosecond) pulses was demonstrated [6] in Xe by 5 fs driving pulses with a 2.3×10^{15} W/cm^2 peak intensity beyond the gas saturation intensity. Numerical modeling of this case showed [6] a radial structure of the bursts dependent on the pulse CEP. Extreme ultraviolet beams were obtained recently [7] in Ar using pulses at 10^{15} W/cm^2 peak power. In these conditions of high ionization a spatially resolved spectral detection allowed the observation of spatiotemporal coupling in the generating medium and a complex spatiospectral structure was observed in the far field. Few-cycle midinfrared pulses are more sensitive to propagation effects and are proposed in Ref. [8] as sources to generate SAPs. Also in this case, reshaping of the fundamental laser field is responsible for the continuum structure in the HHG spectra. Here, SAP is obtained by using a filter centered on axis to select the harmonics in the far field with different divergences.

In this Rapid Communication we numerically demonstrate that in high ionization conditions the LH effect is present in HHG in the gas phase without any special arrangement for the driving pulse. We show that a strong laser pulse interacting with a jet of Ar gas generates attosecond bursts of light with different divergences in successive optical half-cycles, so that in the far field these bunches arrive at different distances from the beam axis. We show that the wave-front curvature, which in Ref. [4] was induced by inserting glass wedges in the beam,

*tosa@itim-cj.ro

here is achieved naturally during beam propagation in a highly ionized gas.

II. METHODS

Numerical calculations have been performed using a nonadiabatic three-dimensional model [9]. The macroscopic gas-phase HHG is described in three main steps: First, it solves the wave equation for the full electric field $E(r,z,t)$ of the laser pulse propagating in a space-time-dependent refractive index in which dispersion from neutral atoms, electron plasma, and the optical Kerr effect are considered; second, it estimates, by using the strong-field approximation [10], the gas polarizability response $P(r,z,t)$ to the propagated field all over the interaction region; finally, it uses the polarizability as a source term to solve the harmonic field propagation equation, again taking into account the frequency-dependent absorption and dispersion. The main result is the harmonic field $H(r,z,t)$ or its frequency counterpart $H(r,z,\omega)$ in the integration domain. Eventually the calculation can be continued by estimating the harmonics in the far field, and in the present investigation it was a necessary part of the modeling.

In developing the model, the main aim is to keep the calculation parameters as close as possible to a physical reality. When dealing with experimental data we start from the measured pulse energy, duration, and chirp or from spectral amplitudes and phases of the laser field, so that the laser pulse is described more realistically, especially when chirped pulses are studied. The focusing conditions as well as the gas density distribution along the propagation direction can be accounted for. No gas distribution is assumed in the transverse direction so that the axial symmetry of the problem is preserved. For Ar atoms the ionization rates were calculated using the Peremolov-Popov-Terentiev model [11] and further ionization of Ar^+ ions was not included in the modeling. Last but not least, we used the quantitative rescattering (QRS) theory [12] in order to improve the strong-field approximation and to account for the energy-dependent cross section of the wave packet at the recombination stage. As shown before [13], including QRS in modeling is essential for Ar as it is known that its photoionization cross section exhibits a so-called Cooper minimum around 47 eV [14], which affects the intensity and phase of the harmonic field.

III. PULSE PROPAGATION IN HIGH IONIZATION CONDITIONS

The case we analyze in the following assumes that laser pulses of 800 nm central wavelength, 1 mJ pulse energy at 21 fs duration generate a peak intensity of 10^{15} W/cm^2 in the focus. For Ar this produces single ionization of all atoms in a region of 40 μm diameter over a 1 mm length of the medium, at 100 Torr gas pressure. In time, this full ionization occurs a few optical cycles before the pulse reaches peak intensity. The dominant component in the space-time-dependent refractive index is the electron plasma contribution, which induces a beam defocusing with a corresponding decrease in intensity. After the full ionization is reached (on axis this takes place around $t = -T_0$, where T_0 is the optical period), the refractive index variation is induced only by the Kerr contribution, which has an effect of a converging lens. In these conditions the leading part of the pulse travels through a medium which strongly defocuses the beam due to the diverging lens created by the electron plasma, while the trailing part gets focused by the optical Kerr effect. The consequence in the temporal structure of the pulse is clearly seen in Fig. 1, where the on-axis field is plotted as a function of time, both initially and after 1 mm. The laser pulse in the early optical cycles travels virtually unaffected, while during the following cycles, $-5T_0 < t < -T_0$, the laser intensity is reduced due to plasma defocusing and self-phase modulation by refractive index variation. Once the ionization is completed, for the following optical cycles the laser pulse exhibits an increase in intensity due to the refractive index variation coming from the Kerr effect.

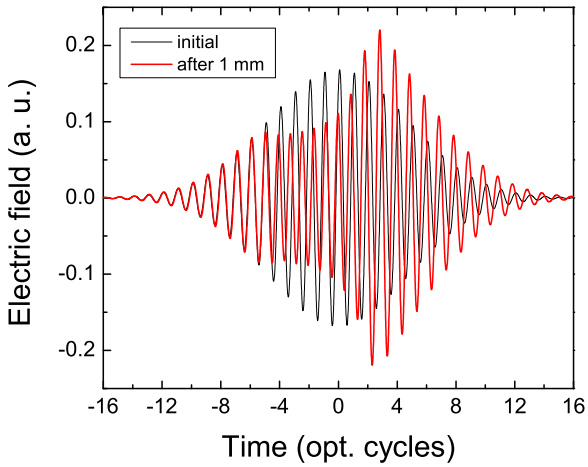

FIG. 1. (Color online) Temporal profiles of an on-axis electric field, initially (black thin line) and after (red, thick line) 1 mm of propagation.

The spatial structure of the laser frequency, represented in an (ω,r) map, at the exit plane is shown in Fig. 2. The same structure at the entrance plane (seen in the inset in Fig. 2) is a Gaussian around the nominal frequency ω_0. At the exit plane close to the on axis (see the region labeled in Fig. 2), the central frequency is split into blueshifted and redshifted components. As r increases, the blueshifted component moves toward the initial frequency of ω_0. An interesting feature reported here is the emergence of a group of frequencies, labeled A and B in Fig. 2. This frequency component, strongly blueshifted on axis, gradually shifts toward lower frequencies as the distance from the beam axis increases from 20 to 80 μm, with a clear spatial chirp: At 20 μm the frequency is centered at $1.14\omega_0$ while at 70 μm it is at $1.04\omega_0$. To complete the characterization of this regime of propagation for the laser field, we calculated the phase derivatives in the axial and radial directions, that is, the axial and radial components of the wave vector. The radial component of the wave vector is close to zero for r close to the beam axis and then sharply increases towards positive values as r increases. For 40 μm $< r <$ 60 μm we estimated an average divergence of 60 mrad, while in the region around the beam axis it is less than 5 mrad. The emerging picture is that the groups of frequencies shown in Fig. 2 propagate along different directions, the on-axis (C) group following the initial

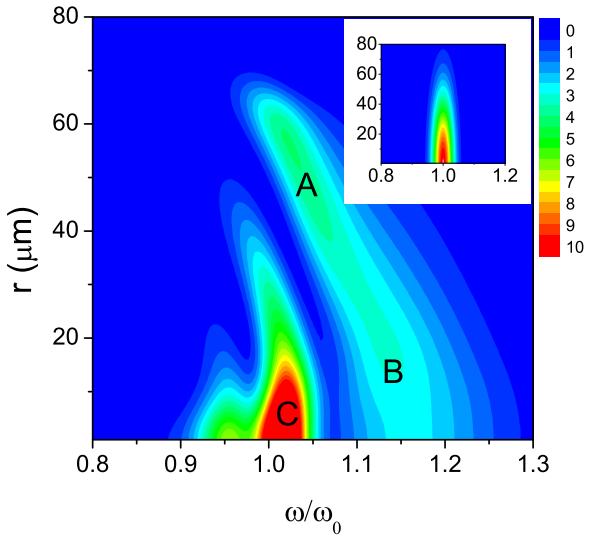

FIG. 2. (Color online) Spatial structure of the laser frequency at the exit plane. The inset shows the Gaussian structure of the laser frequency at the entrance plane.

propagation direction, while the blueshifted groups (A and B) separate and diverge further with r. This wave-front change along the propagation direction is a necessary condition [2–4] for the LH effect to occur.

The spatiotemporal structure of the driving field at the exit plane also can be extracted from the solution $E(r,z,t)$ of the wave equation. The results, shown in Fig. 3(a), reveal the existence of three regions of different intensities, as shown by the isointensity lines generated at 2.8×10^{14} W/cm^2. The earliest one (A) spans between 20 and 60 μm and travels in the leading part of the pulse, having its maximum at three optical cycles before the pulse peak, but extends in time over more than five optical cycles. The B region stretches from on axis to about 30 μm and has a much smaller temporal extension. The most intense one (C) develops around on axis, the increase in intensity being explained in Fig. 1 as due to Kerr focusing. If we represent [Fig. 3(b)] the driving field $E(r,z,t)$ at the exit plane, we have a clear image of the wave-front rotation which takes place at the optical cycle level. In Fig. 3(b) this can be clearly seen in the region labeled A in Fig. 3(a), where we note a continuing change in the wave-front direction from one half-cycle to the next one.

IV. HARMONIC GENERATION

The characteristics of the driving field presented above are expected to be reflected in the generated harmonics. As demonstrated for many other cases (see, for example, Ref. [9]), the generated single dipole response inherits the spatial and spectral features of the driving field. This is valid also for the harmonic field which is a coherent superposition of single dipoles generated all over the interaction region.

We present in Fig. 4 the near-field spatial structure of harmonics from Ar after 1 mm propagation (upper panel) and the corresponding far-field structure (lower panel). For the near field, the similarity between the (ω,r) maps of the driving field and of the harmonic field is obvious. The Cooper

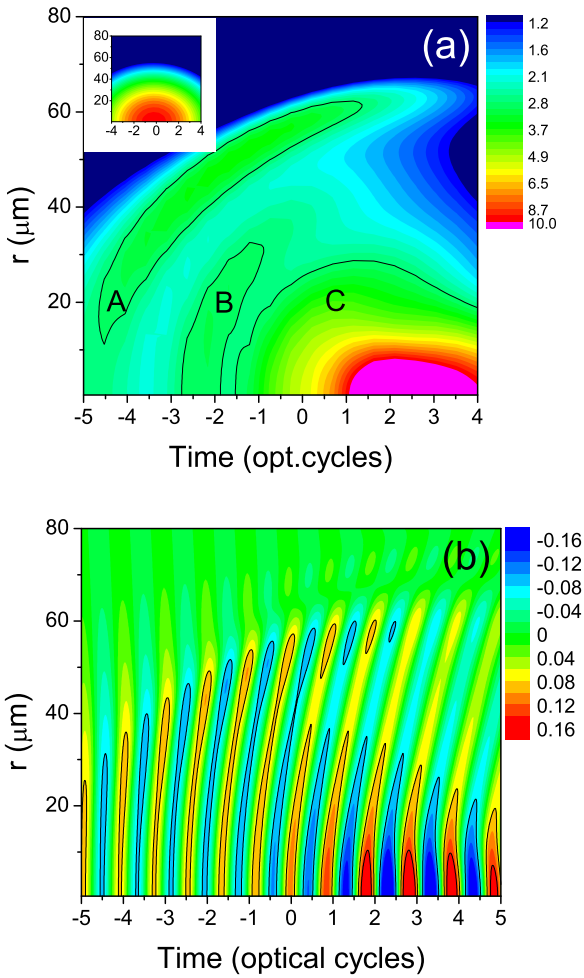

FIG. 3. (Color online) Spatiotemporal structure of the laser pulse at the exit plane. (a) The intensity, in logarithmic scale, is given in units of 10^{14} W/cm^2, and the contour line is for the intensity 2.8×10^{14} W/cm^2. The inset shows the Gaussian structure at the entrance plane. (b) The electric field map (linear scale, atomic units) at the exit plane showing the wave-front rotation along the radial direction at an optical cycle level.

minimum effect is also observable, with harmonic intensities around the 31st order being strongly reduced. However, the far-field pattern clearly departs from the near-field pattern. In the calculations we assumed the far field is collimated by an 80 cm focal length mirror and recorded after the mirror. The reason for the differences seen in Fig. 4 between the near- and far-field structures lies in the emission directions of different spectral components at different radial distances from the axis. Indeed, for harmonic orders over 35, we can observe that the emission arrives at least in three packets, stratified along different emission directions. The central one is confined around on axis, the middle one shines from 1 up to 2.5 mrad, and the last one emits up to 4 mrad. It is interesting to note that the bowed shape of the harmonics showing a quasicontinuum spectral structure is evident, especially for the middle group.

The layered structure of the far field should be put in correspondence with the different directions of emission of the driving field. Indeed, from Fig. 4 we estimate an average half-angle divergence of 1.5–2 mrad for the harmonics around the order

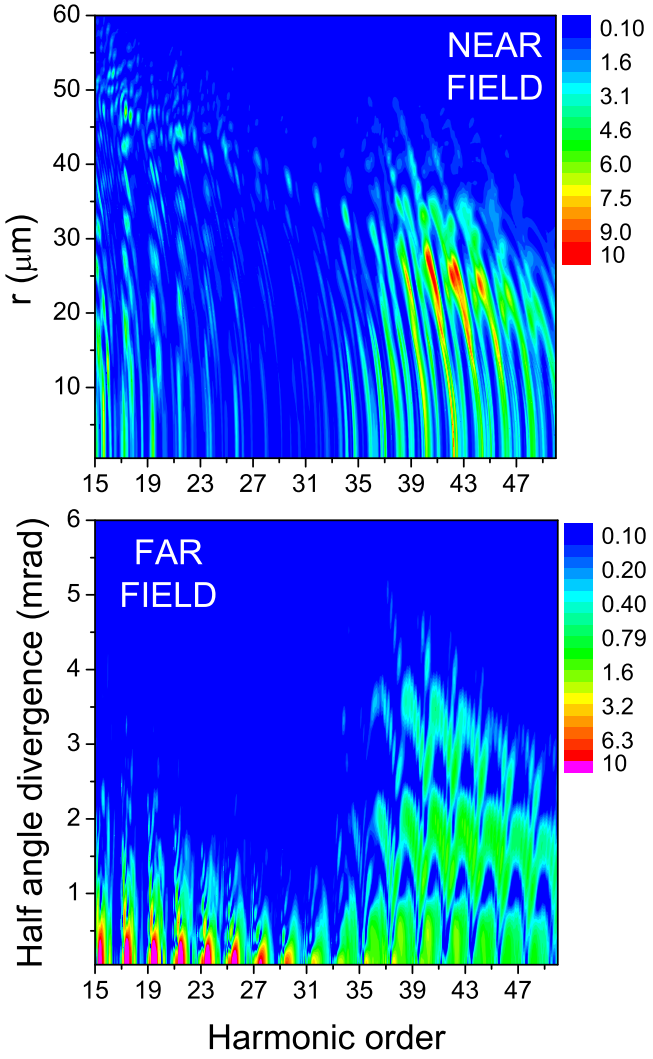

FIG. 4. (Color online) Spatial structure of the harmonics generated in Ar in the near field (after 1 mm of propagation) and in the far field. Logarithmic scales, arbitrary units.

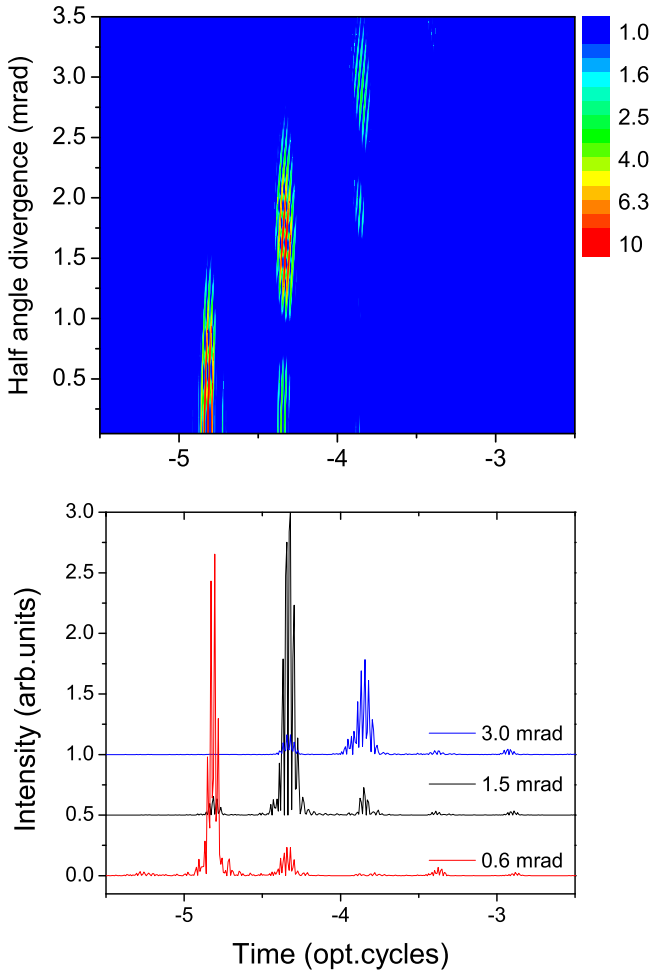

FIG. 5. (Color online) Spatiotemporal structure of the far field emitted by the harmonics from the order 35 to 51, logarithmic scale, arbitrary units. The lower graph shows the temporal structure for three different emission directions.

40, meaning a half angle of emission for the driving field of 60–80 mrad, in agreement with the value found for the region A in Fig. 2. On the other hand, the quasicontinuum structure observed for the harmonics over the order 35 should be put in correspondence with the field intensity in the two (A and B) groups of wavelets seen in Figs. 2 and 3. Indeed, the laser intensity in regions A and B in Fig. 3 is below 3×10^{14} W/cm^2, which corresponds to a cutoff order around 51 for Ar.

Finally, we show in Fig. 5 the time counterpart of the far-field spectral structure shown in Fig. 4. The spectrum for each wavelet was filtered from the order 35. As expected, in time we see bursts of radiation separated by half an optical cycle. The stratified structure along the radial direction seen in the frequency domain is maintained in the time domain as well, so we can see that the earliest burst of radiation is emitted close to on axis, as seen in the lower panel of Fig. 5. A second strong burst is emitted half a cycle later with a half angle of 1.5 mrad. Finally, a third burst is emitted along a direction which makes a 3 mrad angle with the axis. The three main emissions are followed in time by a couple of weaker satellites, so each group has a quasisingle attosecond pulse structure.

We note that a similar spatiotemporal structure of bursts was obtained in Ref. [6] by modeling the interaction of 5 fs pulses at 2.3×10^{14} W/cm^2 with Xe gas. Figure 5 in Ref. [6] shows successive attosecond bursts emitted in successive half-cycles at increasing distance from the axis, their structure being dependent on the CEP of the driving field. For CEP $= 0$ an on-axis attosecond pulse is followed by two weaker bursts at larger divergence, while for CEP $= \pi/2$ two successive attosecond pulses were obtained on axis and more bursts in the following half-cycles at different off-axis positions. It is difficult to estimate whether the same spatiotemporal configuration was established during propagation for the few-cycle driving field. Though the peak intensity and medium length are similar (2.5 mm), the pressure is much lower (2.5–3 Torr) and the propagation regime could be different for these two cases.

V. CONCLUSIONS

We present numerical results which demonstrate that the lighthouse effect occurs in HHG from Ar in highly ionizing

conditions. We analyze the structure of the driving field in time, frequency, and space, and conclude that the complete ionization of Ar on axis gives rise to additional wavelets at off-axis regions. We show that these wavelets propagate with increasing divergence as r increases, generating the rotation of the wave front, fulfilling a necessary condition for the LH effect to occur. These wavelets have enough intensity (in Fig. 3 the contour of laser intensity 2.8×10^{14} W/cm^2 means a cutoff around the order 51 in Ar) to induce a harmonic field structure which for frequencies close to the cutoff exhibit a layered structure in the radial direction. In time, the harmonic emission consists of successive pulses separated by a half-period and propagating with different divergences from the interaction region. The lighthouse effect here is generated naturally in the HHG process, and is a consequence of the spatial structure of the driving field in this particular propagation regime.

The LH effect in highly ionizing gas media would be quite a universal phenomena so that similar spatiotemporal configurations for the LH effect could be obtained with various driving laser and medium conditions. For example, our additional calculations show that, for the configuration presented here, the LH effect is present for a range of gas pressures from 50 to 150 Torr. Also, the driving field wavelength is not restricted to 800 nm—midinfrared wavelengths can also induce similar spatiotemporal configurations, provided enough intensity is available. The basic ingredient for LH effect is that the spatiotemporal configuration of the refractive index, mainly induced by ionization, provides a spatial chirp of a driving laser pulse during propagation.

ACKNOWLEDGMENTS

We thank Kyung Taek Kim for useful suggestions and discussions. The authors acknowledge support from the Institute for Basic Science under IBS-R012-D1. V.T. acknowledges support from the Ministry of Science, ICT and Future Planning, and from Romanian Financing Authority CNDI-UEFISCDI under Project No. PN II-ID-PCE-2012-4-0342.

[1] F. Krausz and M. Y. Ivanov, Rev. Mod. Phys. **81**, 163 (2009).
[2] H. Vincenti and F. Quere, Phys. Rev. Lett. **108**, 113904 (2012).
[3] J. A. Wheeler, A. Borot, S. Monchocé, H. Vincenti, A. Ricci, A. Malvache, R. Lopez-Martens, and F. Quéré, Nat. Photonics **6**, 829 (2012).
[4] K. T. Kim, C. Zhang, T. Ruchon, J.-F. Hergott, T. Auguste, D. M. Villeneuve, P. B. Corkum, and F. Quere, Nat. Photonics **7**, 651 (2013).
[5] B. Zeng, W. Chu, G. Li, J. Yao, J. Ni, H. Zhang, Y. Cheng, Z. Xu, Y. Wu, and Z. Chang, Phys. Rev. A **85**, 033839 (2012).
[6] F. Ferrari, F. Calegari, M. Lucchini, C. Vozzi, S. Stagira, G. Sansone, and M. Nisoli, Nat. Photonics **4**, 875 (2010).
[7] A. Dubrouil, O. Hort, F. Catoire, D. Descamps, S. Petit, E. Mével, V. V. Strelkov, and E. Constant, Nat. Commun. **5**, 4637 (2014).
[8] C. Jin, A.-T. Le, C. A. Trallero-Herrero, and C. D. Lin, Phys. Rev. A **84**, 043411 (2011).
[9] V. Tosa, H. T. Kim, I. J. Kim, and C. H. Nam, Phys. Rev. A **71**, 063807 (2005); **71**, 063808 (2005).
[10] M. Lewenstein, P. Balcou, M. Y. Ivanov, A. L'Huillier, and P. B. Corkum, Phys. Rev. A **49**, 2117 (1994).
[11] A. M. Perelomov, V. S. Popov, and M. V. Terentev, Sov. Phys. JETP **23**, 924 (1966).
[12] A. T. Le, R. R. Lucchese, S. Tonzani, T. Morishita, and C. D. Lin, Phys. Rev. A **80**, 013401 (2009).
[13] C. Jin, H. J. Wrner, V. Tosa, A.-T. Le, J. B. Bertrand, R. R. Lucchese, P. B. Corkum, D. M. Villeneuve, and C. D. Lin, J. Phys. B: At., Mol. Opt. Phys. **44**, 095601 (2011).
[14] J. W. Cooper, Phys. Rev. **128**, 681 (1962).